Particle Impact Analysis of Bulk Powder During Pneumatic Conveyance

Report Contributors: Giles Richardson[1], Mark Cooker[2], Niamh Delaney[3], Kevin Hanley[4], Poul Hjorth[5], Dana Mackey[6], Joanna Mason[3,7], Sarah Mitchell[3] and Catherine O'Sullivan[8]

Industry Representative: Seamus O'Mahony[9]

[1]School of Mathematics, University of Southampton, United Kingdom
[2]School of Mathematics, University of East Anglia, United Kingdom
[3]MACSI, Department of Mathematics and Statistics, University of Limerick, Ireland
[4]Department of Process and Chemical Engineering, University College Cork, Ireland
[5]Department of Mathematics, Technical University of Denmark, Denmark
[6]School of Mathematical Sciences, Dublin Institute of Technology, Ireland
[7]Report coordinator, joanna.mason@ul.ie
[8]Department of Civil and Environmental Engineering, Imperial College London, United Kingdom
[9]Wyeth Nutritionals Ireland, Askeaton, Co. Limerick, Ireland

Abstract

Fragmentation of powders during transportation is a common problem for manufacturers of food and pharmaceutical products. We illustrate that the primary cause of breakage is due to inter-particle collisions, rather than particle-wall impacts, and provide a statistical mechanics model giving the number of collisions resulting in fragmentation.

1 Introduction

Pneumatic conveyance of food and pharmaceutical products in dehydrated, powdered form, is very common in Ireland's process industries. During conveyance, powder particles may break into smaller pieces, due to impacts, resulting in a change in overall bulk density. A leading manufacturer of infant formula approached the 70th European Study Group with Industry to investigate the change in bulk density that they observe during transportation of this powder.

The powder is inhomogeneous and consists of approximately six main ingredients, and around twenty additional micro-nutrients, which are smaller particles. An average particle is approximately spherical and around 100 microns in diameter. Particles consist of proteins, sugars and fats and can be either solid or hollow. If hollow, the size of the wall is typically one fifth of the diameter, and the walls can be solid or porous see Figure 1a.

Initially the powder is produced from a liquid in the spray dryer. During this phase the particles can coalesce into clusters (see Figure 1b), which is desirable as agglomerates of particles are better at dissolving in water, when reconstituting the infant formula. The particles are blown along pipes by an air flow, and then intermediately stored in silos, before packing into cans. During transportation particles impact both the walls of the pipe and also each other. A schematic diagram of an industrial pneumatic conveyance line is shown in Figure 2. Typical parameters for both the particles, and the pneumatic conveyance line are listed in Table 3.

Infant formula is usually measured out by volume using a scoop. Therefore bulk density of the powder is an essential quality control parameter for infant formula manufacturers. If there is too much breakage during transportation, the average size of the particle clusters decreases because the particles can pack together more tightly, and as a result the bulk density increases. This results in the formula becoming too nutrient rich when reconstituted. Conversely, if there is unusually little breakage during transportation, the final bulk density could be too low, and the rehydrated formula will be insufficient in meeting the infant's nutritional requirements.

As a certain amount of breakage during transportation is inevitable, manufacturers currently estimate the change in bulk density from empirical data. The aim of the study group is to devise a mathematical model for the amount of breakage during transportation, and thus quantify the bulk density change.

The purpose of this report is twofold: to outline the main mechanisms of impact, and to provide an analytical expression for the rate of particle breakage during transportation. The outline is as follows. We begin in Section 2 by describing Dean flow, which is the standard way of describing flow in a curved pipe. In Sections 3 and 4 we consider particle flow in the pipe. We initially consider a toy two-dimensional problem, and then extend our analysis to the full three-dimensional problem. An overview of Hertzian contact laws, which we can use to estimate the energy at which particle impacts result in fracture, is presented in Section 5. For Hertzian theory to apply, it is assumed that the impacting bodies are solid. In Section 5.2 we outline an argument to illustrate that the walls of the particles under consideration are sufficiently thick that we may justifiably model them as solid. Section 6 focuses on constructing a statistical

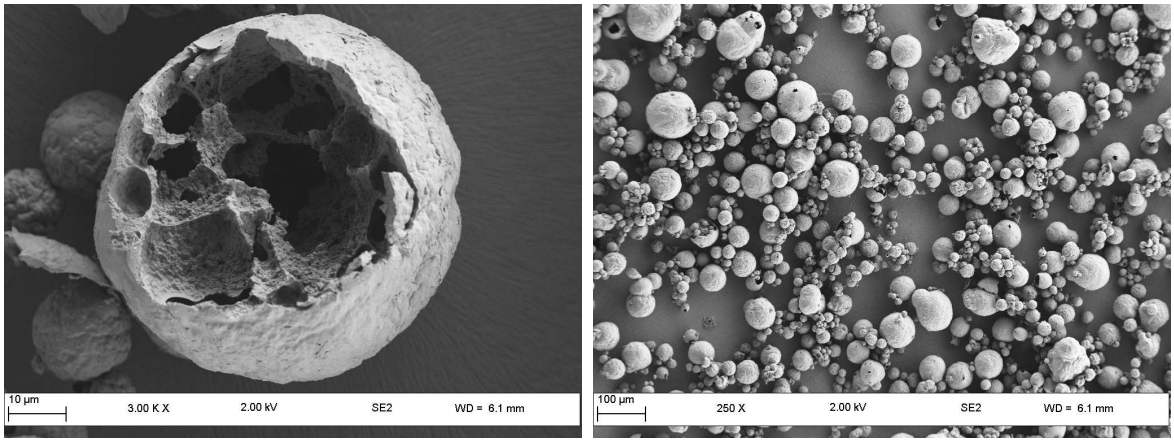

Figure 1: SEM images of a typical particle and clusters of particles. A scale bar is shown below each image. Photographs reproduced with permission from Kevin Hanley.

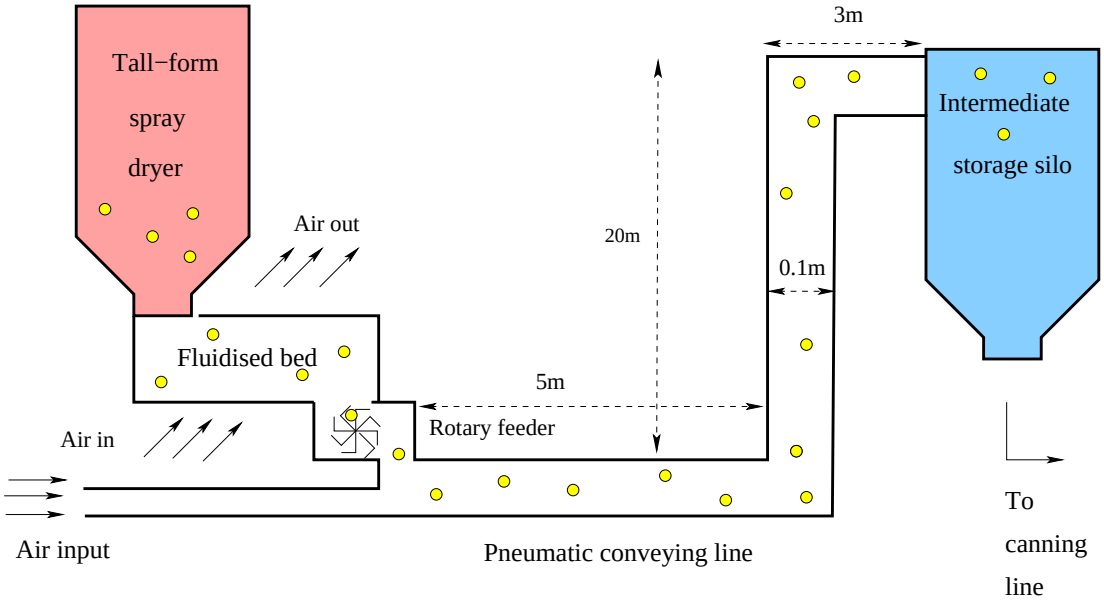

Figure 2: A schematic diagram of an industrial pneumatic conveyance line for the transport of infant formula from the spray drying phase to the storage silos.

Quantity	**s**ymbol	**v**alue(s)	**u**nits
Particle radius	a_0	5×10^{-6}–5×10^{-4}	m
Radius of pipe	R	0.05	m
Radius of curvature of pipe	κ_0	1	m
Estimated density of particles in the pipe	ρ	250–350	kg/m^3
Estimated velocity of particles in the pipe	v_0	0.5–1	m/s
Poisson's ratio	ν	0.3	-
Young's Modulus	E	3×10^9 (from [10])	Pa
Coefficient of restitution	-	0.2	-
Yield stress	σ_f	5×10^5	Pa

Table 3: Typical particle and pipe parameters provided by Kevin Hanley, unless otherwise stated.

mechanics model of collisions resulting in fragmentation, which implicitly incorporates Hertzian theory. Finally, in Section 7 we provide some concluding remarks and outline areas for future work.

2 The flow in the pipe

The pipe has an approximately circular cross-section and has a centreline that is weakly curved (*i.e.* has typical radius of curvature $L \gg 2\sigma$ where 2σ is the diameter of the pipe cross section. Flow in curved pipes is usually described as a Dean flow [4] and reviewed in [3]. Such flows are characterised by the *so-called* Dean number De and δ the ratio of the typical pipe radius (or half-width in the case of non-circular pipes) σ to its typical radius of curvature L. Unfortunately the Dean number is not defined in the same manner in all works. Here we shall adopt the definitions

$$\mathrm{De} = \frac{\rho G \sigma^3 (2\sigma/L)^{1/2}}{\mu^2}, \qquad \delta = \frac{\sigma}{L}, \tag{2.1}$$

where G is a typical pressure gradient along the pipe, μ is the viscosity of the fluid and ρ its density. At low Dean numbers (below about 100) this definition is equivalent to another commonly used definition namely

$$\hat{\mathrm{De}} = 4\mathrm{Re}\left(\frac{2\sigma}{L}\right)^{1/2} \qquad \text{where the Reynolds number} \quad \mathrm{Re} = \frac{2\sigma\rho\bar{W}_0}{\mu}, \tag{2.2}$$

where $\bar{W}_0$ is the mean velocity along the pipe. However these two definitions do not coincide for larger Dean numbers.

At low Dean numbers $De \ll 1$, and for loosely coiled pipes $\delta \ll 1$, the flow is, to a good approximation, a Poiseuille flow along the axis of the pipe with a small circulatory component in the transverse cross-section of the pipe. In the study group we initially made the assumption that significant flow (as far as motion of particles in the flow is concerned) occurs mainly in the axial direction. However, as we shall briefly outline here, this assumption is probably invalid so that further investigation should be directed to considering flow in the cross-section of the pipe. In fact the high Dean number limit turns out to be of more relevance to the flows in the conveyance line than the low Dean number limit.

The structure of the flow at high Dean number. The high Dean number limit has been considered previously by [5, 6, 14] by using a mixture of numerical and asymptotic techniques. They define the flow velocity $\mathbf{u} = w\mathbf{t} + v(\sin\alpha\mathbf{b} - \cos\alpha\mathbf{n}) + u(\cos\alpha\mathbf{b} + \sin\alpha\mathbf{n})$ (here $\mathbf{t}$ is the unit vector along the axis of the pipe, $\mathbf{n}$ is the unit vector in the plane of the pipe centreline directed towards the inside of the this curve, $\mathbf{b}$ is the other unit normal vector (see Figure 3)). In the limit $De \gg 1 \quad \delta \gg 1$ [5, 6, 14] have shown that in the bulk of the flow the scalings for the various velocity components are

$$u = O\left(De^{1/3}\frac{\nu}{\sigma}\right), \quad v = O\left(De^{1/3}\frac{\nu}{\sigma}\right), \quad w = O\left(De^{2/3}\frac{\nu}{\sigma}\left(\frac{L}{2\sigma}\right)^{1/2}\right). \tag{2.3}$$

In addition they identify a boundary layer of thickness $O(\sigma De^{-1/3})$ around the edge of the pipe in which the solution is such that

$$u = O\left(De^{2/3}\frac{\nu}{\sigma}\right), \quad v = O\left(De^{1/3}\frac{\nu}{\sigma}\right), \quad w = O\left(De^{2/3}\frac{\nu}{\sigma}\left(\frac{L}{2\sigma}\right)^{1/2}\right). \tag{2.4}$$

At these high Dean numbers the Dean number is related to the mean axial velocity $\bar{W}$ by (2.3c), that is by

$$De = O\left(\frac{\bar{W}^{3/2}\sigma^{9/4}}{\nu^{3/2}L^{3/4}}\right). \tag{2.5}$$

Here we give no further details of this solution except to say that it has to be calculated numerically, even in the boundary layer.

Turbulent pipe flow. The conveyance line flow occurs at high Reynolds number. So for example, we estimated the Reynolds number as 20,000 by taking the viscosity of the flow to be that of air. In practice the net viscosity of the mixture of air and particles will be more than this, so the Reynolds number will be less than for air alone. Nevertheless the flow may still be turbulent. The boundary layer structure of a turbulent flow in a straight pipe is described to a reasonable approximation by the *so-called* Law of the Wall (see for example [1, 16]). It is less clear however what the equivalent structure is in a curved pipe.

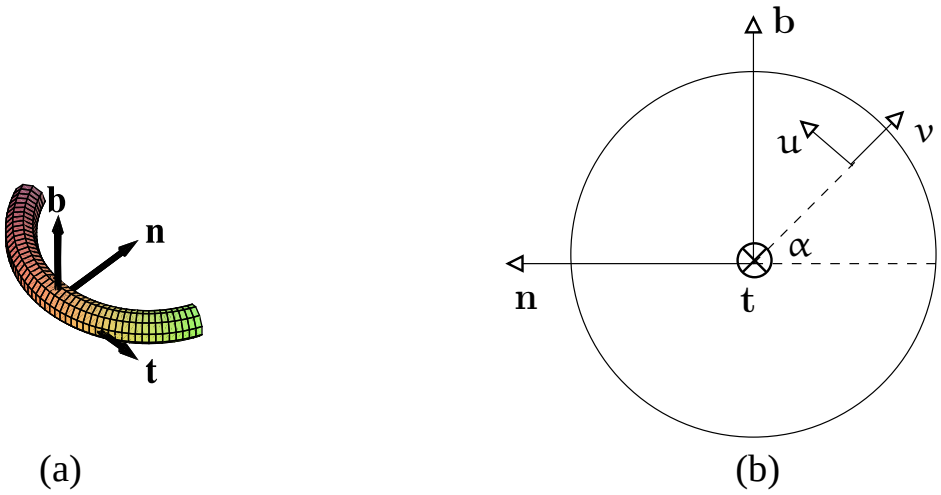

Figure 3: Illustration of the coordinates used to describe the flow in the pipe. Panel (a) shows the definitions of the vectors $\{\mathbf{t}, \mathbf{n}, \mathbf{b}\}$ while panel (b) shows the definition of the velocity components (here $\mathbf{t}$ is directed into the paper).

3 Can collisions of particles with the wall of the pipe account for particle fragmentation?

Here we consider particle motion in the pipe flow. Since particles are small such motion is usually dominated by the fluid drag, rather than inertia. This motivates us to ask the question can particles ever collide with the side of the pipe with sufficient velocity in order to cause their fragmentation (*i.e.* velocities of $\mathsf{O}(1\mathrm{ms}^{-1})$)? In particular we note that it is the centrifugal force on the particle that is likely to be the cause of motion across streamlines towards the edge of the pipe and, further, that since the flow velocity at the boundary of the pipe is zero we would not expect the centrifugal force on a particle close to the edge of the pipe to be large. However it is still possible to envisage a situation in which there is a narrow boundary layer in the vicinity of the pipe wall, across which the fluid velocity drops rapidly to zero, where the particle has sufficient inertia to cross from the region of high fluid velocity to the pipe wall without losing most of its kinetic energy. In order to investigate this possibility we will consider the toy problem of a particle moving in a two-dimensional flow.

3.1 The 2D problem

Here we consider a toy two-dimensional problem noting that where the two-dimensional boundary layer structure is similar to that of the real flow the resulting particle trajectories will be qualitatively similar. Since the particle Reynolds number is typically small we can approximate

its equation of motion by balancing particle inertia against linear Stokes drag to give

$$m\frac{d^2\boldsymbol{x}}{dt^2} = 6\pi\mu r_p\left(\boldsymbol{v} - \frac{d\boldsymbol{x}}{dt}\right). \tag{3.1}$$

Here m is the mass of one particle, r_p is the radius of the particle, $\boldsymbol{x}$ and $\boldsymbol{v}$ are the position and velocity of the particle respectively, and μ is the fluid viscosity. Note that the Stokes drag formula is assumed because the flow of air relative to the moving particle has a low (local) Reynolds number, quite different from the high Re for the air flow down the pipe.

We would like to consider two particular scenarios. In the first (i) the particle moves in a pipe flow around a circular bend in which the predominant flow is in the direction of the tangent to the centreline $\mathbf{t}$ (*i.e.* takes the form $\boldsymbol{u} = w\mathbf{t}$). The second scenario (ii) aims to model the situation where the secondary Dean flows in the cross-section of the pipe are of more significance to particle-wall collisions than the primary flow along the axis of the pipe. In order to model these situations we introduce polar coordinates for the particle describing its position by $\boldsymbol{x} = R(t)\boldsymbol{e}_r$ so that, on differentiation with respect to t we find

$$\dot{\boldsymbol{x}} = \dot{R}\boldsymbol{e}_r + R\dot{\theta}\boldsymbol{e}_\theta, \qquad \ddot{\boldsymbol{x}} = (\ddot{R} - R\dot{\theta}^2)\boldsymbol{e}_r + (2\dot{R}\dot{\theta} + R\ddot{\theta})\boldsymbol{e}_\theta,$$

where $\boldsymbol{e}_r$ and $\boldsymbol{e}_\theta$ are the unit radial and azimuthal vectors in the coordinate directions of the plane polars r and θ, whose origin is at the pipe centreline. Furthermore in both scenarios (i) and (ii) the flow is predominantly in the azimuthal direction; this motivates us to write $\boldsymbol{v} = g(R,\theta)\boldsymbol{e}_\theta$.

We non-dimensionalise (3.1) by writing

$$\boldsymbol{x} = R_0\boldsymbol{x}^*, \quad R = R_0R^*, \quad \boldsymbol{v} = V_0\boldsymbol{v}^*, \quad t = \frac{R_0}{V_0}t^*,$$

which gives, on dropping $'*$s, substituting $\boldsymbol{x}^* = R^*\boldsymbol{e}_r$ and equating components in the radial and azimuthal directions,

$$\ddot{R} - R\dot{\theta}^2 = -\tilde{\Gamma}\dot{R}, \qquad 2\dot{R}\dot{\theta} + R\ddot{\theta} = \tilde{\Gamma}(g(R,\theta) - R\dot{\theta}). \tag{3.2}$$

where

$$\tilde{\Gamma} = \frac{6\pi\mu r_p R_0}{mV_0}.$$

In scenario (i) we are typically interested in a pipe with radius of curvature which is much greater than the pipe radius whereas in scenario (ii) we are interested in flow occurring in a narrow boundary layer around the edge of the pipe. This suggests that we should further write $R = 1 - \varepsilon z$ where $R = 1$ denotes the outer edge of the pipe and where the small parameter $\varepsilon = \frac{X_{bl}}{R_0}$ gives the ratio of the boundary layer thickness to the typical radius of curvature of the

pipe. On making this substitution in (3.2), writing $\dot{\theta} = \Omega$ and on rescaling time by writing $t = \varepsilon\tilde{\Gamma}\tau$ we obtain the following system

$$\frac{dz}{d\tau} = -(1-\varepsilon z)\Omega^2 - \Upsilon\frac{d^2z}{d\tau^2} \tag{3.3}$$

$$\Upsilon\left((1-\varepsilon z)\frac{d\Omega}{d\tau} - 2\varepsilon\Omega\frac{dz}{d\tau}\right) = \hat{g}(z,\theta) - (1-\varepsilon z)\Omega \tag{3.4}$$

$$\frac{d\theta}{d\tau} = \varepsilon^{1/2}\Upsilon^{-1/2}\Omega. \tag{3.5}$$

where $\Upsilon = \varepsilon^{-1}\tilde{\Gamma}^{-2}$. The key parameter in this problem is Υ (recall that $\varepsilon \ll 1$). This parameter corresponds to the ratio of to the timescale for drag to accelerate a particle to the velocity of the flow to that for a particle to traverse the boundary layer. Thus if $\Upsilon \ll 1$ the particle moves, to a good approximation, with the velocity of the flow. If however $\Upsilon = O(1)$ the particle can cross the boundary layer to the wall of the pipe without being decelerated to almost zero velocity at the wall. In other words if $\Upsilon \ll 1$ it will impact the wall (at $z = 0$) with very small velocity (an asymptotic analysis reveals that the dimensionless velocity normal to the wall on impact will at most be $O(\Upsilon^2)$ corresponding to a dimensional velocity of at most $O(V_0\varepsilon^{1/2}\Upsilon^{5/2})$). For $\Upsilon = O(1)$, however, the particle impacts the wall with $O(1)$ dimensionless velocity normal to the wall corresponding to a dimensional velocity of $O(V_0\varepsilon^{1/2})$. [10]

In summary we expect that the chance of particle impacts on the wall leading to particle fracture is negligible if

$$\Upsilon = \frac{m^2V_0^2}{(6\pi\mu r_p)^2R_0X_{bl}} \ll 1,$$

where X_{bl} is the width of the flow boundary layer and R_0 is the typical radius curvature of the problem (in case (i) flow along the axis of the pipe R_0 is the typical radius of curvature of the pipe centreline while in case (ii) in which secondary flows dominate the process R_0 is the radius of the pipe) . Where $\Upsilon = O(1)$ the particle impacts the wall with a velocity of $O(V_0\varepsilon^{1/2})$ and there is a significantly greater chance of particle fracture on impact. Even where $\Upsilon \ll 1$ inter-particle collisions give another possible mechanism giving rise to particle fracture. This will be considered further in §4.

Relevance to Dean flow. Consider first the flow along the pipe, parallel to its centreline, corresponding to case (i). Here we can identify R_0 with the radius of curvature of the pipe centreline L, the velocity can be read off from (2.3c) and (2.4c) so that the key parameters are

$$R_0 = L, \qquad V_0 = De^{2/3}\frac{\nu}{\sigma}\left(\frac{L}{2\sigma}\right)^{1/2}, \qquad X_{bl} = \sigma De^{-1/3},$$

[10]Note that where $\Upsilon \gg 1$ the asymptotic analysis reveals an inertial particle trajectory in which both w and $dz/d\tau$ are unchanged to leading order; in order to retain more information it is necessary to rescale distance normal to the boundary to give an $O(1)$ value of Υ.

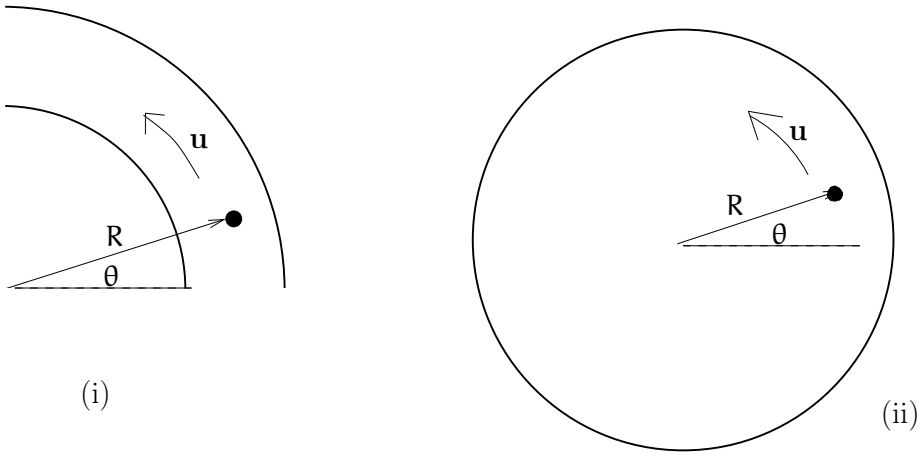

Figure 4: The flows considered for the toy problem

and thus give

$$\Upsilon = \frac{m^2\nu^2}{(6\pi\mu r_p)^2}\frac{De^{5/3}}{2\sigma^4} \qquad \text{in case (i).} \tag{3.6}$$

In case (ii) we can identify R_0 with the radius of the pipe σ, while the typical velocity is that in the azimuthal direction (which can be read off from (2.4a)). The key parameters are thus

$$R_0 = \sigma, \qquad V_0 = De^{2/3}\frac{\nu}{\sigma}, \qquad X_{bl} = \sigma De^{-1/3},$$

from which it follows that

$$\Upsilon = \frac{m^2\nu^2}{(6\pi\mu r_p)^2}\frac{De^{5/3}}{\sigma^4} \qquad \text{in case (ii).} \tag{3.7}$$

We can relate these expressions for Υ to the mean axial velocity in the pipe $\bar{W}$ via (2.5). It is immediately apparent that Υ is the same order of magnitude in both cases signifying that the azimuthal and longitudinal velocities occurring in Dean flow have comparable effects on the motion of particles across the boundary layer adjacent to the pipe boundary. Thus any quantitative analysis requires that we consider the full three-dimensional problem (rather than the toy model treated here).

4 Particle transport in the pipe

The particle Reynolds number is relatively small and so we can approximate drag force by the linear Stokes relation. Balancing inertia with the drag force gives

$$m\frac{d^2\mathbf{x}}{dt^2} = 6\pi\mu a\left(\boldsymbol{\nu} - \frac{d\mathbf{x}}{dt}\right), \tag{4.1}$$

where a is the radius of the particle, $\mathbf{x}$ and $\boldsymbol{\nu}$ are the position and velocity of the particle respectively, and μ is the fluid viscosity.

Since the radius of the pipe is generally considerably smaller than its radius of curvature it is helpful to introduce a local coordinate system based about the centre line of the pipe, $\mathbf{r} = \mathbf{q}(s)$, defined by

$$\mathbf{x} = \mathbf{q}(s) + \xi\mathbf{n}(s) + \eta\mathbf{b}, \tag{4.2}$$

where $\mathbf{n}(s)$ and $\mathbf{b}$ are the principal unit normal and unit binormal vectors respectively, s measures arclength along the centre line, and $\sqrt{\eta^2+\xi^2}$ measures the distance of the point from the centre line.

We use the standard Serret-Frenet formulae (see, for example [12]) to relate the various quantities in (4.2), namely

$$\frac{d\mathbf{q}}{ds} = \mathbf{t}, \qquad \frac{d\mathbf{t}}{ds} = \kappa\mathbf{n}, \qquad \frac{d\mathbf{n}}{ds} = \tau\mathbf{b} - \kappa\mathbf{t}, \tag{4.3}$$

where κ is the pipe curvature, τ is the torsion and $\mathbf{t}$ is the tangent vector. To make the equations complete we also have $d\mathbf{b}/dt = \tau\mathbf{n}$. We assume a planar pipe and so $\tau = 0$, therefore in the subsequent analysis we can ignore the $\mathbf{n}$ component of the equations of motion.

In order to track an individual particle at position $\mathbf{x}(t)$ we rewrite (4.2) as $\mathbf{x}(t) = \mathbf{q}(s(t)) + \xi(t)\mathbf{n}(s(t)) + \eta\mathbf{b}$ and use (4.1) to find differential equations for ξ and s. Before substituting $\mathbf{x}(t)$ into (4.1) we nondimensionalise by choosing

$$\begin{aligned} &\mathbf{x} = \frac{\mathbf{x}^*}{\kappa_0}, \quad \mathbf{q} = \frac{\mathbf{q}^*}{\kappa_0}, \quad r = Rr^*, \quad \eta = R\eta^*, \quad \kappa = \kappa_0\kappa^*, \\ &\xi = R\xi^*, \quad a = a_0a^*, \quad t = \frac{t^*}{\kappa_0\nu_0}, \quad \boldsymbol{\nu} = \nu_0\boldsymbol{\nu}^*, \quad s = \frac{s^*}{\kappa_0}, \end{aligned} \tag{4.4}$$

where R is the radius of the pipe, κ_0 is the typical curvature of the pipe centreline, a_0 is a typical particle radius and ν_0 is a typical fluid velocity. On dropping the $*$'s the dimensionless equations (4.1) and (4.2) become

$$\frac{d^2\mathbf{x}}{dt^2} = \frac{\Gamma}{a^2}\left(g(r)\mathbf{t} - \frac{d\mathbf{x}}{dt}\right), \tag{4.5}$$

and

$$\mathbf{x} = \mathbf{q}(s) + \epsilon(\xi\mathbf{n}(s) + \eta\mathbf{b}), \tag{4.6}$$

where we have assumed that the flow is primarily parallel to the centreline of the pipe and has the nondimensional form $\boldsymbol{\nu} = g(r)\mathbf{t}$, with $r = \sqrt{\eta^2 + \xi^2}$. We assume that the coordinate η is constant while the particle moves. Note that equation (4.3) remains unchanged.

The dimensionless parameters in (4.5) and (4.6) are given by

$$\Gamma = \frac{9\mu}{2a_0^2\nu_0\kappa_0\rho}, \qquad \epsilon = R\kappa_0. \tag{4.7}$$

Typical sizes of these parameters, using Table 3, are $\Gamma \approx 11$ and $\epsilon \approx 0.1$, which allows us to set $\Gamma = \gamma/\epsilon$ where $\gamma = O(1)$.

Using the Serret-Frenet equations (4.3) we differentiate $\mathbf{x}$ in (4.6) to give

$$\frac{d\mathbf{x}}{dt} = \dot{s}(1 - \epsilon\xi\kappa)\mathbf{t} + \epsilon\dot{\xi}\mathbf{n} \tag{4.8}$$

$$\frac{d^2\mathbf{x}}{dt^2} = \left[\ddot{s}(1 - \epsilon\xi\kappa) - \epsilon\dot{s}\left(2\dot{\xi}\kappa + \xi\frac{d\kappa}{ds}\dot{s}\right)\right]\mathbf{t} + \left[\kappa(1 - \epsilon\xi\kappa)\dot{s}^2 + \epsilon\ddot{\xi}\right]\mathbf{n}. \tag{4.9}$$

Upon substitution into (4.5) and equating coefficients of $\mathbf{t}$ and $\mathbf{n}$ we obtain the following equations relating ξ and s

$$\ddot{s}(1 - \epsilon\xi\kappa) - \epsilon\dot{s}\left(2\dot{\xi}\kappa + \xi\frac{d\kappa}{ds}\dot{s}\right) = \frac{\gamma}{\epsilon a^2}[g(r) - \dot{s}(1 - \epsilon\xi\kappa)] \tag{4.10}$$

$$\kappa(1 - \epsilon\xi\kappa)\dot{s}^2 + \epsilon\ddot{\xi} = -\frac{\gamma}{a^2}\dot{\xi}. \tag{4.11}$$

Assuming $n\epsilon \ll 1$ we find that the leading order terms satisfy

$$\dot{s} = g(\sqrt{\eta^2 + \xi^2}), \qquad \dot{\xi} = -\frac{a^2\kappa(s)}{\gamma}\dot{s}^2. \tag{4.12}$$

Eliminating $\dot{s}$ gives the expression

$$\dot{\xi} = -\frac{a^2\kappa(s)}{\gamma}\left[g(\sqrt{\eta^2 + \xi^2})\right]^2, \tag{4.13}$$

or in dimensional form

$$\dot{\xi} = -\frac{2a^2\kappa(s)\nu_0^2\rho}{9\mu}\left[g(\sqrt{(\eta/R)^2 + (\xi/R)^2})\right]^2. \tag{4.14}$$

Further work could treat a particle on the median plane $\eta = 0$. Also quite generally, since $g(r = 1) = 0$ at the wall, we can at least be sure that $\frac{d\xi}{dt}$ decreases to zero as the particle approaches the wall. Although we can't set $g(r) = 1 - r^2$, because the Reynolds number is high, such a dependence in the boundary layer near $r = 1$ tells us that $1 - r = 1 - \xi(t)$ (on $\eta = 0$) decreases to zero with exponential decay, hence there is no impact velocity.

5 Hertz theory for binary collisions

5.1 Critical Energy

Hertz theory is an analysis of stresses at the contact of elastic solids. It was initially developed for static loading, but subsequently extended to quasi-static impacts (e.g. of spheres). We use Hertz theory to give an estimate for the critical energy, i.e., the energy needed to break a given particle of some radius a, here we give a brief overview of the key equations.

As in [15], consider a (collinear) collision between two particles, modelled as smooth, homogeneous, solid, elastic spheres, of radii a_1 and a_2 respectively. The elastic properties of the spheres are given by their Young moduli E_i and Poisson's ratios ν_i ($i = 1, 2$). We look at a quasi-static process and thus consider an instant where the mutual force of compression is P. The spheres compress elastically, with a contact area of radius a_c, see Figure 5.

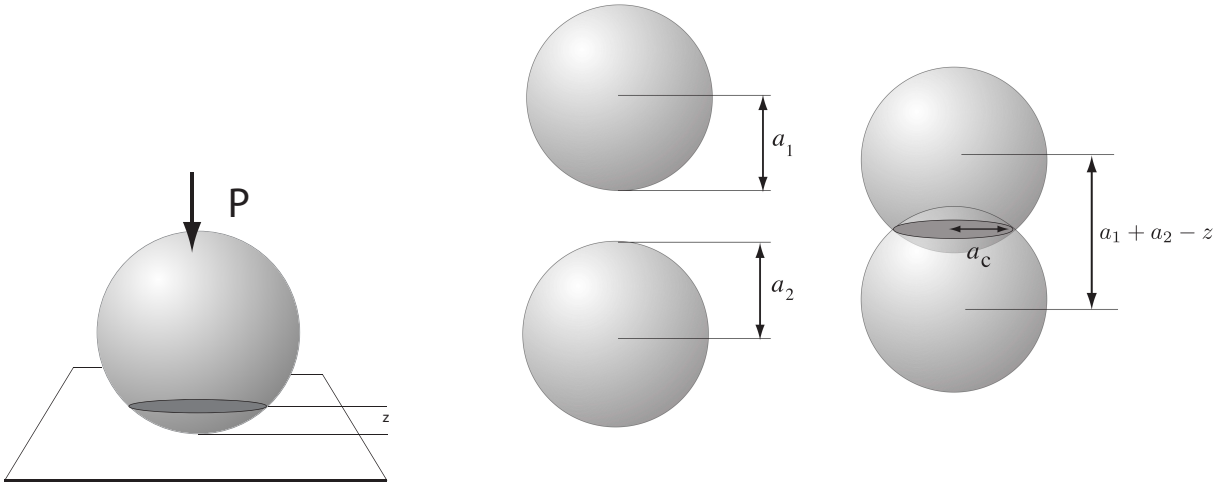

Figure 5: From left to right: elastic sphere forced onto an elastic plane with a force P, and two spherical particles of radii a_1 and a_2 colliding collinearly. z is the amount of compression, and a_c is the radius of the contact disk.

The distribution of pressure across the contact area, as a function of distance r away from the centreline, is

$$p = p(r) = p_0 \left[1 - \left(\frac{r}{a_c} \right) \right], \tag{5.1}$$

where a_c is the radius of the contact zone between the particles, and the maximum pressure p_0 is given by

$$p_0 = \frac{3P}{2\pi a_c^2}. \tag{5.2}$$

The effective values of the Young's modulus E^* and radius a^* are defined via

$$\frac{1}{E^*} = \frac{1-{\nu_1}^2}{E_1} + \frac{1-{\nu_2}^2}{E_2}, \qquad \text{and} \qquad \frac{1}{a^*} = \frac{1}{a_1} + \frac{1}{a_2},$$

respectively.

From Hertz theory, we then have the following relations between the applied force P, the effective Young's modulus E^*, the effective radius a^*, and the compression distance z:

$$P = \frac{4}{3} E^* a^{*1/2} z^{3/2}, \tag{5.3}$$

where z is given by $a_c^2 = a^* z$, and

$$a_c = \left(\frac{3Pa^*}{4E^*} \right)^{\frac{1}{3}}. \tag{5.4}$$

The critical compression distance, at which fracture occurs, is denoted z_f. For a collision that just reaches this critical compression length z_f, the work done by the compression force just equals the initial kinetic energy E_r, and thus:

$$E_r = \frac{1}{2} m V_f^2 = \int_0^{z_f} P(z) dz. \tag{5.5}$$

V is the relative impact velocity, and V_y is defined as the yield velocity. Provided $V < V_y$ the interaction is assumed to be elastic. Inserting the above expression for $P(z)$ we get

$$E_r = \frac{8}{15} \frac{E^* z_f^5}{a^{*2}}, \tag{5.6}$$

We can relate the critical compression distance z_f to the contact yield stress σ_f of the material by

$$\sigma_f \equiv p_0(z_f),$$

From equation (5.2) and (5.3) we have

$$\sigma_f = \frac{2E^* z_f}{\pi a^*}. \tag{5.7}$$

Rearranging for z_f, and substituting this expression into (5.5) we obtain the energy at which the particle is estimated to fracture:

$$E_r = \frac{\pi^5}{60} \frac{a^{*3} \sigma_f^5}{E^{*4}}. \tag{5.8}$$

We shall return to this expression in Section 6, where we shall consider the statistics of particle collisions leading to fragmentation.

5.2 Particle structure

Hertz theory, as mentioned in the previous section, assumes that the two impacting spheres are solid. However, the particles that make up infant formula, see Figure 1 are clearly hollow. The study group was asked to investigate how far into the particle there are significant increases in stress, and therefore whether modelling the spheres as hollow should be incorporated into the model. Here, we consider the simpler case of two impacting cylinders, although it should be straightforward to extend the result to two spheres.

Recall that z is the distance from the contact point. If we take the origin of the z-axis to be at the point where the two cylinders first contact, then $z = 0$ is the location of a plane of contact between the two cylinders i.e., the point at which the contact force is distributed over a rectangle of width $2a_c$ and length equal to the length of the shortest cylinder. This is the smallest possible area over which the contact force is distributed, and therefore the point at which the stress has its maximum value.

As the compression increases, the rectangular area becomes larger, because the width of the rectangle constantly increases due to the curvature of the circular cross-section. Since stress is force/area, the stresses decrease as z increases.

From [7] we have an expression for σ_z, the stress in the z direction

$$\frac{\sigma_z}{p_0} = -\frac{a_c}{\sqrt{a_c^2 + z^2}}, \tag{5.9}$$

where p_0 is the maximum pressure, and for two cylinders in contact is given by $p_0 = \left(\frac{PE^*}{\pi R}\right)^{\frac{1}{2}}$ (see [7]). (Note that the convention in mechanical engineering is to take compressive stresses to be negative.)

In Figure 6 we plot a graph of the stress divided by the maximum pressure $(\frac{\sigma_z}{p_0})$ against the distance from the contact point, za_c, for a constant a_c and typical particle parameters.

At $z = 0$, the compressive stress is at its maximum. We also observe that the stresses diminish extremely rapidly as you move further away from the contact point. We expect an entirely analogous result in the case of two impacting spheres. If the stress changes are non negligible at a depth that is close to the wall thickness, then Hertz theory is not applicable. If the extent of the zone where there is a measurable increase in stress is small, then Hertz theory can be used to represent the contact mechanics of these particles. As the walls of the infant formula particles are approximately a fifth of the diameter, we conclude that approximating the particles as solid spheres is a reasonable assumption.

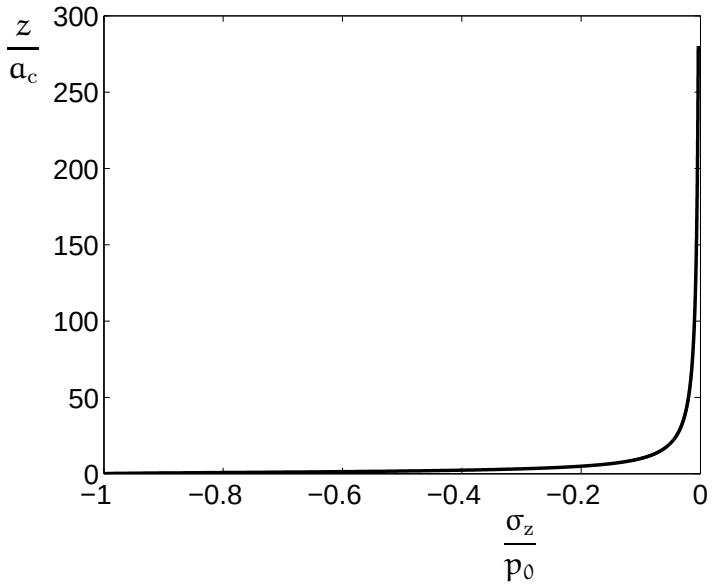

Figure 6: We consider two cylinders in contact. The graph shows the stress divided by the maximum pressure ($\frac{\sigma_z}{p_0}$) plotted against the distance from the contact point, ($\frac{z}{a_c}$), for a constant a_c.

6 The statistics of collisions leading to fragmentation

Consider a particle size distribution such that the proportion of particles with radius lying in the range $(a, a + da)$ is $n(a)da$. Furthermore take the probability of breaking a particle of size a when it undergoes a collision in which an energy in the range $(E, E + dE)$ is released to it is $p_b(E, a)dE$. We note that at present both these distributions will have to be derived from experiment, though an ultimate goal of this type of work might be to formulate a Smoluchowski model of the evolution of the size distribution $n(a)$.

In §4 we calculated the transverse velocity $\dot{\xi}$, due to centrifugal force, of a particle being advected in a curved pipe as a function of its radius. Notably this was proportional to the square of the radius of the particle (bigger particles travel more quickly than smaller ones). We also saw that this velocity slowed markedly as the particle approached the outer edge of the pipe, a consequence of the slowing of the flow along the pipe in the immediate vicinity of the pipe wall. This lead us to conclude that collisions of particles with the pipe wall give rise to insignificant particle fragmentation and to hypothesise that the main cause of particle breakage is collisions between particles of different radii travelling with different transverse velocities $\dot{\xi}$. It is the aim of this section to quantify this process.

We start by considering the total number of collisions between particles of sizes in the range $(a, a+da)$ with those in the range $(\alpha, \alpha+d\alpha)$. In the direction of the principle normal $\mathbf{n}$ they approach each other with velocity $|\dot{\xi}(a)-\dot{\xi}(\alpha)|$, see Figure 7. Since they will only collide if their

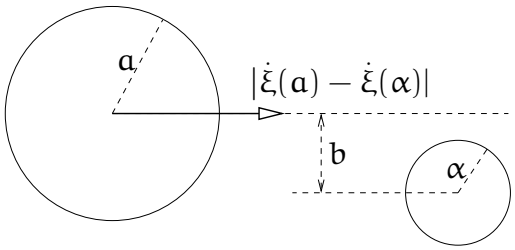

Figure 7: A schematic diagram of a particle with radius a approaching a particle with radius α. b denotes the distance between their centres, and $|\dot{\xi}(a) - \dot{\xi}(\alpha)|$ their approach velocity.

centres come within a distance $(a+\alpha)$ of each other the average number of collisions occurring to a particle of radius a with particles with radii in the range $(\alpha, \alpha + d\alpha)$ in a small time dt is $N\pi(a+\alpha)^2|\dot{\xi}(a) - \dot{\xi}(\alpha)|n(\alpha)d\alpha dt$, where N is the total number density of all particles. It follows that

$$\left(\begin{array}{l} \text{The number of collisions in time } dt \text{ per unit} \\ \text{volume between particles with radii in range } (a, a+da) \\ \text{with those with radii in range } (\alpha, \alpha + d\alpha) \end{array} \right) = N^2\pi(a+\alpha)^2|\dot{\xi}(a) - \dot{\xi}(\alpha)|n(\alpha)n(a)d\alpha da dt$$

Of these collisions we need to work out how many lead to fracture. We have already calculated the energy released in an impact between a particle radius a and one with radius α when their centres are offset by a distance b (see Figure 7). Such collisions release energy

$$E_r(a, \alpha, b) = \frac{1}{2}\left(\frac{m(a)m(\alpha)}{m(a)+m(\alpha)}\right)(v(a) - v(\alpha))^2\left(1 - \frac{b^2}{(a+\alpha)^2}\right).$$

Of this we hypothesise that the energy divides between the particles proportional to their mass, that is

$$\text{Energy available for fracture of particle } a = \frac{m(a)}{m(a)+m(\alpha)}E_r(a, \alpha, b), \tag{6.1}$$

$$\text{Energy available for fracture of particle } \alpha = \frac{m(\alpha)}{m(a)+m(\alpha)}E_r(a, \alpha, b), \tag{6.2}$$

where E_r is the energy at which the particle is estimated to fracture, and is given in Section 5. The fraction of collisions for which the offset distance between the centres of the particles (at collision) lies in $(b, b+db)$ is $(2\pi b db)/(\pi(a+\alpha)^2)$ (see Figure 8b) and the energy released in such a collision is $E_r(a, \alpha, b)db$.

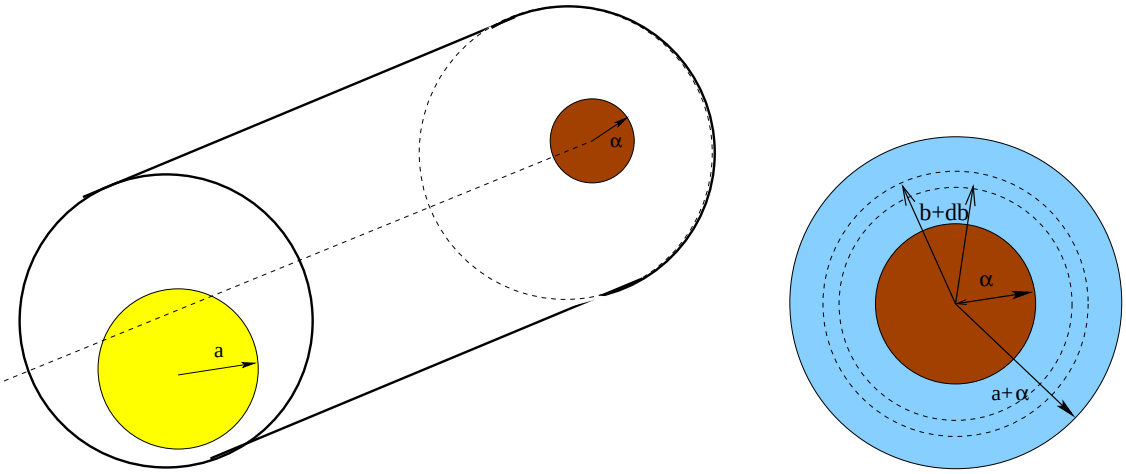

Figure 8: Here the first figure shows a large particle of size a approaching a smaller particle size α. The second figure shows the end view of the cylinder with the smaller particle lying at the centre. Provided the centre of the larger particle (with radius a) lies within the cylinder the particles will collide.

Referring to (6.2) we find that

$$\begin{aligned}&\text{Number of particles size}\\&\text{range } (a, a+da) \text{ per unit time } = N^2\pi\int(a+\alpha)^2|\dot{\xi}(a)\\&\text{per unit volume which fracture}\end{aligned}$$

$$-\dot{\xi}(\alpha)|n(a)n(\alpha)\left[\int_0^{E_{max}} p_b\left(\frac{m(a)}{m(a)+m(\alpha)}E_r\right) d\left(\frac{m(a)}{m(a)+m(\alpha)}E_r\right)\right] d\alpha. \quad (6.3)$$

Translating (6.3) into terms of the separation b between the particle centres (perpendicular to the velocity) upon impact this can be written as

$$\begin{aligned}\text{Fracture rate} &= \begin{array}{l}\text{Number of particles size}\\ \text{range } (a, a+da) \text{ per unit time } = F(a,x)\\ \text{per unit volume}\end{array}\\ &= N^2\pi\int_0^\infty \frac{m(a)(a+\alpha)^2}{m(a)+m(\alpha)}|\dot{\xi}(a,x)\\ &\quad -\dot{\xi}(\alpha,x)|n(a)n(\alpha)\left[\int_0^{a+\alpha} p_b\left(\frac{m(a)}{m(a)+m(\alpha)}E_r(a,\alpha,b)\right)\frac{\partial E_r}{\partial b}db\right] d\alpha. \quad (6.4)\end{aligned}$$

7 Conclusions

We have provided a model for the flow in the curved pipe which we used to show that the velocity of particles decreases rapidly as they approach the pipe wall. We believe that particle-

wall collisions give rise to insignificant particle fragmentation, and that the main mechanism for particle breakage is collisions between particles of different sizes.

We have analysed inter-particle collisions, using Hertzian contact laws to provide a criterion for when a binary collision leads to breakup. In addition we have justified modelling these particles as solid, rather than hollow. Finally, we used a statistical mechanics approach to generate an expression for the total rate of particle breakup in the flow.

Future work would involve experimental verification of this model.

Acknowledgements

This work was carried out at the 70th European Study Group with Industry, hosted by the Mathematics Applications Consortium for Science and Industry (MACSI), funded by the Science Foundation Ireland (SFI) Mathematics initiative 06/MI/005. We would like to thank William Lee for his comments on an earlier draft.

Bibliography

[1] P. Bradshaw and G.P. Huang, The Law of the Wall in turbulent flow, *Proc. Roy. Soc. Lond. A* **4**51, 165–188, (1995).

[2] N.V. Brilliantov, F. Spahn, J-M. Hertzsch, T. Pöschel, The collision of particles in granular systems. *Phys. A*, **3**21, 417–424, (1996).

[3] S.A. Burger, L. Talbot and L.-S. Yao, Flow in curved pipes. *Ann. Rev. Fluid Mech.* **1**5, 461–512, (1983).

[4] W.R. Dean, The stream-line motion of fluid in a curved pipe. *Phil. Mag.* **5**, 673 (1928).

[5] S.C.R. Dennis and N. Riley, On the fully developed flow in a curved pipe at large Dean number. *Proc. R. Soc. Lond. A* **4**34, 473–478, (1991).

[6] H. Ito, Laminar flow in curved pipes. *Z. agnew Math. Mech.* **4**9, 653–663, (1969).

[7] K.L. Johnson, *Contact Mechanics*, Cambridge University Press, (1985).

[8] F. Kun and H.J. Herrmann, Transition from damage to fragmentation in collision of solids. *Phys. Rev. E*, **5**9, 3, (1999).

[9] T.J. Pedley, Mathematical modelling of arterial fluid dynamics. *J. Eng. Math.* **4**7, 419–444, (2003).

[10] M. Perkins, S.J. Ebbens, S. Hayes, C.J. Roberts, C.E. Madden, S.Y. Luk, N. Patel, Elastic modulus measurements from individual lactose particles using atomic force microscopy. *Int. J. Pharm.*, **3**32, 168–175, (2007).

[11] T. Pöschel and N. Brilliantov (editors), *Granular Gas Dynamics*, Springer Lecture Notes in Physics, (2003).

[12] John Roe, *Elementary Geometry*, Oxford University Press, (1993).

[13] J.H. Siggers and S.L. Waters, Steady flow in pipes with finite curvature. *Phys. Fluids* **1**7, 077102 (2005).

[14] F.T. Smith, Steady motion within a curved pipe. *Proc. R. Soc. Lond. A* **3**47, 345–370, (1976).

[15] C. Thornton, Coefficient of restitution for collinear collisions of elastic-perfectly plastic spheres. *J. Appl. Mech.*, **6**4, 383–386, (1997).

[16] http://www.maths-in-industry.org/miis/105/